Softening of the Symmetric Breathing Mode in Gold Particles by Laser-Induced Heating†

Gregory V. Hartland* and Min Hu

Department of Chemistry and Biochemistry, 251 Nieuwland Science Hall, University of Notre Dame, Notre Dame, Indiana 46556-5670

John E. Sader

Department of Mathematics and Statistics, The University of Melbourne, Victoria 3010, Australia

Received: December 3, 2002; In Final Form: January 10, 2003

The symmetric breathing mode in spherical gold particles has been examined by time-resolved spectroscopy using different intensity pump laser pulses. The results show that the period of the breathing mode increases as the pump laser power increases, up to pump laser powers of 2−3 μJ/pulse. This is attributed to softening of the elastic properties of the particles due to laser-induced heating. At pump laser powers greater than ∼3 μJ/pulse the period versus intensity data flatten off. This most likely arises from saturation of the sample absorption at high pump intensities. The particles studied in these experiments were relatively large—between 50 and 100 nm in diameter. Large particles were chosen because they have slower heat dissipation times, which means that the temperature in the particles is better defined during the course of the experiment. The particle temperatures were estimated from the laser power density, the heat capacity of gold, and the absorption at the pump wavelength—assuming that the samples obey Beer's law. This allows us to compare the experimental results to calculations of the period versus temperature, which are based on the known temperature-dependent elastic constants of gold. The experimental and calculated periods are in excellent agreement up to the melting point of gold, which is predicted to occur at ∼3 μJ/pulse (approximately the same point where the period versus intensity data flatten off). At higher powers the measured periods are significantly shorter than those predicted for molten gold particles. This implies that we can approach the melting point of gold, but we cannot completely melt the particles. Analysis of the damping of the beat signal indicates that we may form solid-core/liquid-shell particles at high laser powers.

1. Introduction

The interaction of light with colloidal metal particles has been a major area of interest in physical chemistry since Faraday's pioneering experiments.[1] Recently the use of metal particles for biomolecule detection,[2,3] plasmon propagation in metallic wires,[4−6] and optical limiting applications[7,8] has continued to make the spectroscopy of metal particles an important area of research. A useful way of studying the optical properties of metal particles is time-resolved spectroscopy.[9−13] In these experiments the pump laser primarily acts to heat the electron distribution of the particle.[14] The electrons subsequently equilibrate with the phonon modes, and the time scale for this process provides information about the electron−phonon coupling constant.[15−17] This sudden lattice heating can also coherently excite the phonon mode that correlates with the expansion coordinate, which for spherical particles is the symmetric breathing mode.[12,13] The coherently excited phonon mode appears as a modulation in transient absorption experiments. The period of the modulation depends on the speed of sound and size of the particles.[18,19] In turn the speed of sound depends on the density and elastic moduli of the material.[20] Thus, experiments that detect these modulations provide a way of investigating the material properties of nanometer-sized objects, which is difficult to do by conventional techniques.

The systems that have been examined to date by time-resolved techniques include spherical silver,[18] gold,[19] gallium and tin particles,[21] bimetallic gold−lead particles,[22] ellipsoidal silver particles,[23] rod-shaped gold particles,[24] and (very recently) aggregated gold particles.[25] Semiconductor nanoparticles of PbS,[26] PbTe,[27] and InAs[28] have also been investigated. In almost all cases the measured period is exactly the same as that predicted by continuum mechanics calculations. The exceptions are the very small <2 nm InAs particles,[28] and the gold nanorod experiments of ref 24. For the InAs particles the deviation from predicted behavior is presumably due to the size dependence of the elastic constants of the material.[28] On the other hand, for the gold nanorods a satisfactory theory that describes the vibrational response of finite cylinders to impulsive heating does not exist at present.

The majority of these experiments have been performed with relatively low pump laser fluences, so that the increase in the temperature of the lattice is several hundred kelvin at most.[29] However, it is relatively easy to provide pump laser pulses with enough power to melt or even fragment the particles.[30−38] The aim of this paper is to examine how the period and damping time of the coherently excited phonon modes change with pump laser intensity, using fluences that provide sufficient energy to (potentially) melt the particles.

The particles chosen for this study are relatively large, with diameters on the order of 100 nm. Large particles were chosen for three reasons: (i) Large particles have better size distribu-

† Part of the special issue "Arnim Henglein Festschrift".

* To whom correspondence should be addressed. E-mail: hartland.1@nd.edu.

10.1021/jp0276092 CCC: $25.00 © 2003 American Chemical Society
Published on Web 03/06/2003

tions,[39,40] which is an important consideration for these experiments. (ii) For metal particles in solution the time scale for heat dissipation scales as R^2, so that large particles have much slower heat dissipation times.[41] This means that the temperature is better defined over the time of our experiments for large particles. (iii) At very high laser intensities the modulations are hard to observe for small particles, because the time scale for lattice heating becomes similar to the period of the symmetric breathing mode.[19] This tends to "wash-out" the coherent response of the particle. The results from our experiments show that we can achieve very high lattice temperatures—approaching the melting point of bulk gold. However, based on the way the measured period changes with intensity, we do not believe that we have melted the particles. This may be because of saturation of the pump laser absorption at high power, or because these materials take a finite time to melt after heat deposition. These experiments show that time-resolved spectroscopy is a powerful technique for measuring the material properties of nanometer-sized objects—under conditions far from room temperature and pressure.[42] These results are also relevant to understanding laser-induced heating and heat dissipation in nanostructures, as well as optical limiting effects in metal particles.[7,8]

2. Experimental Procedures

The time-resolved experiments were performed with a regeneratively amplified Ti:sapphire laser system that has been described in detail elsewhere.[43] Pump pulses at 400 nm were produced by doubling the fundamental from the Ti:sapphire laser, and probe pulses in the visible region were obtained from a white light continuum. The intensity of the pump pulses was controlled with a $\lambda/2$-waveplate/polarizer combination. The pump laser intensity at the sample was measured by a Molectron J3-02 energy detector, and the pump laser spot size was $(3.0 \pm 0.5) \times 10^{-4}$ cm^2 for these experiments. The laser spot size was measured by observing the color change in a thin film of citrate-stabilized gold particles. The film changes color from the characteristic purple of interacting particles to red under laser irradiation, due to laser-induced melting and fusion of neighboring particles.[44] Specific probe wavelengths were selected using a Jobin-Yvon Spex H-10 monochromator (10 nm spectral resolution) placed after the sample. Fluctuations in the probe intensity were normalized using a simple analogue division circuit.[43] The wavelength of the probe laser was chosen to give the clearest signal from the coherently excited vibrational modes. The exact wavelength depends on the particular sample being examined.

Intensity-dependent measurements show that the pump laser absorption follows Beer's law up to pump laser powers of $\sim$3 μJ/pulse, which corresponds to a fluence of $\sim$10 mJ/cm^2. Higher pump laser fluences produce nonlinear effects such as self-focusing and (eventually) white light generation in the sample. All the pump laser intensities given in this paper correspond to incident intensities. In the temperature calculations reported below we have corrected for the reflection at the front window of the cell. (The error that arises from neglecting the reflection correction is much smaller than the error from the uncertainty in the laser spot size at the sample.)

The experimental data were fitted using a damped cosine function, $S(t) = a_1 \cos(2\pi t/\tau_R + \phi) \exp[-(\Gamma_\sigma t)^2] + a_2 \exp(-t/\tau_2) + a_3$, using the "Solver" routine in Microsoft Excel. In this equation τ_R is the period corresponding to the average-sized particle in the sample (see eq 3 below), Γ_σ is the damping constant due to polydispersity in the sample, and the last two terms account for the "background" signal. Assuming that the sample has a Gaussian distribution of sizes, the damping due to polydispersity is given by $\Gamma_\sigma = (\sqrt{2})\pi\sigma_R/\bar{R}\tau_R$, where $\bar{R}$ is the average size and σ_R is the standard deviation.[29] This analysis assumes that the dephasing of the modulations is dominated by inhomogeneous damping; that is, there is no contribution from pure dephasing processes such as energy transfer to the environment.

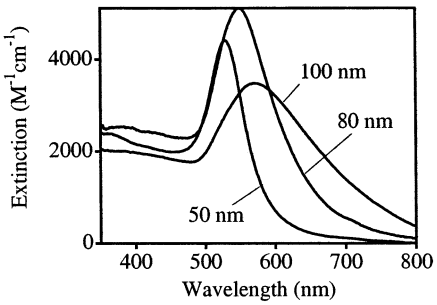

Figure 1. UV−vis absorption spectra of the gold colloids used in this study. The average size is given in the figure. Note that the spectra have been scaled using the experimental data presented in refs 39 and 40.

Three different samples with average diameters of 51 nm ($\sigma_R/\bar{R} = 9\%$), 82 nm ($\sigma_R/\bar{R} = 5\%$), and 104 nm ($\sigma_R/\bar{R} = 6\%$) were examined in this study. These particles were made by depositing gold onto the surface of seed particles via radiation chemistry.[39,40] The seed particles used were 15 nm diameter gold particles, which were prepared using the standard citrate reduction recipe.[45] All the samples were in aqueous solution, and the particles were stabilized by adsorbed citrate anions. The concentration of gold was approximately 2×10^{-4} M for all the solutions. The particle size distributions were determined from the quantum beat signal using the analysis described above. The average size was confirmed by TEM analysis of the samples. UV−vis absorption spectra were recorded on a Perkin-Elmer Lambda 6 UV−vis spectrophotometer. For the transient absorption measurements, the samples were held in 2 mm cuvettes and the experiments were performed without flowing. At high powers the heat deposited by the pump laser causes a significant decrease in the density of the solvent. This creates small convection "plumes" which, fortuitously, mix the sample and help avoid laser-induced degradation.

3. Experimental Results

UV−vis extinction spectra of the different particles are presented in Figure 1. The spectra have been scaled according to the data presented in refs 39 and 40. There are several important points to note from Figure 1. First, the plasmon band shifts to the red and becomes broader for the larger particles.[46,47] This broadening is not due to increased polydispersity. Specifically, for a given sample time-resolved experiments performed with the same pump power and different probe wavelengths give identical values for the period and damping time, to within experimental error. This implies that the differently sized particles in the sample have virtually identical spectra. This is significantly different from our recent experiments with gold nanorods, where we found that the period strongly depends on the probe wavelength.[24] For the nanorods the probe wavelength dependence of the period arises because different length rods in the sample have different spectra; the position of the longitudinal plasmon band depends on the aspect ratio of the rod.[48] Second, there is a slight decrease in the extinction coefficient in the UV region for the larger particles. For metal particles, the extinction arises from both scattering and absorp-

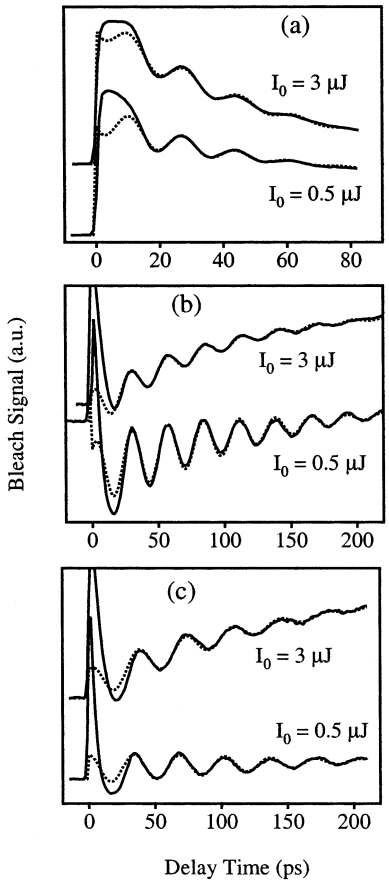

Figure 2. Transient bleach data for the different gold colloid samples recorded with pump laser intensities of 0.5 and 3 μJ/pulse: (a) 50 nm diameter particles; (b) 80 nm diameter particles; (c) 100 nm diameter particles. Note the different time axes for (a) compared to (b) and (c).

tion and, in general, the scattering contribution increases with size.[46,47] Thus, the slight decrease in extinction for the 100 nm particles implies a significant decrease in the molar absorption coefficient. This is an important consideration for the temperature calculations presented below.

Representative transient absorption traces for the different samples used in the experiments are shown in Figure 2. The two traces in each panel correspond to experiments performed with 0.5 and 3 μJ energy pump laser pulses, and the signals have been normalized at approximately 0 ps delay time. Also shown are fits to the data using a damped cosine function. Note the different scales for the time axis for the larger particles in Figure 2. All the traces show the same general features: a fast initial decay that corresponds to the transfer of energy from the electrons to the phonons (most noticeable in Figure 2b,c), and modulations due to the coherently excited breathing mode.[12,13] The higher intensity data also show an increasing bleach signal at longer times.[43] Note that the characteristic cooling times for these particles are expected to be ~400 ps for the 50 nm diameter particles, 1000 ps for the 80 nm particles, and 1600 ps for the 100 nm particles.[41] These time scales are much longer than the time scale of the experiment. Using the results of ref 41, we estimate that the temperature decreases by less than 20% during the course of the experiment. Thus, heat dissipation to the environment is not a major concern in these measurements.

Figure 3 shows the period of the modulations versus the incident pump laser intensity for the different samples. Again there are some general features to note. The measured period increases with intensity up to $I_o \approx 2-3$ μJ/pulse, and then flattens off at higher power. At higher powers it becomes more

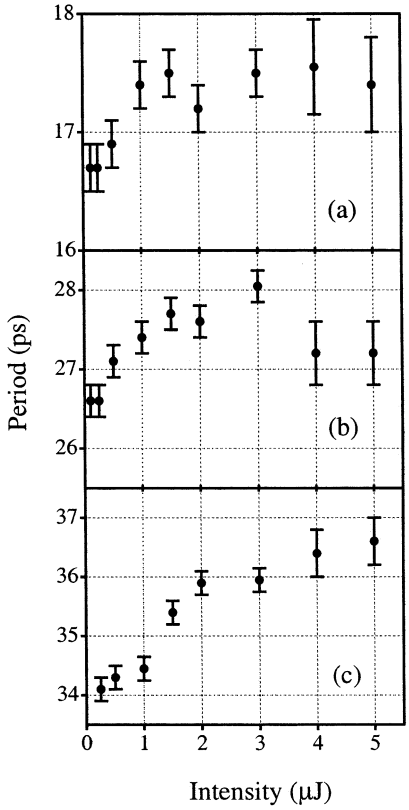

Figure 3. Period of the coherently excited breathing mode versus pump laser power for the gold colloid solutions: (a) 50 nm diameter particles; (b) 80 nm diameter particles; (c) 100 nm diameter particles.

difficult to accurately fit the data and extract the modulation period. This is primarily due to the rising background in the transient bleach signal. Because of the interference from this signal, it is also difficult to accurately measure the decay time of the modulations at high power (vida infra). It is interesting to note that the point where the period versus intensity data flatten off is about the same for each sample. This "threshold" is also approximately the same power where we start to observe nonlinear effects in the pump beam transmission. The level of excitation in the particles is best quantified by the number of photons absorbed per gold atom (n). This can be calculated using Beer's law, and for our experimental conditions (pump laser spot size and wavelength), $n \approx 0.04I_o$, where I_o is the pump laser intensity (here in microjoules). Thus, the point where the period versus intensity data flatten off corresponds to an excitation level of ~10%. Note that this estimate assumes that the samples obey Beer's law at these powers, and that the absorption coefficient for gold at 400 nm is 1800 M^{-1} cm^{-1}.

In Figure 4 the periods extracted from the transient absorption experiments are plotted versus temperature. The temperature in the particles was estimated from the pump laser intensity (I_o), the spot size (σ), the absorbance of the sample at 400 nm, and the heat capacity (C_p) and enthalpy of fusion (ΔH_{fus}) of gold. Specifically, the heat deposited into the particles q (J mol^{-1}) is

$$q = 2.303(I_o/\sigma)\alpha_{400} \quad (1)$$

where α_{400} is the absorption coefficient (M^{-1} cm^{-1}) for the sample. The temperature rise in the particle is calculated from q by

$$q = \int_{T_0}^{T} C_p(s)\, dT \quad (2a)$$

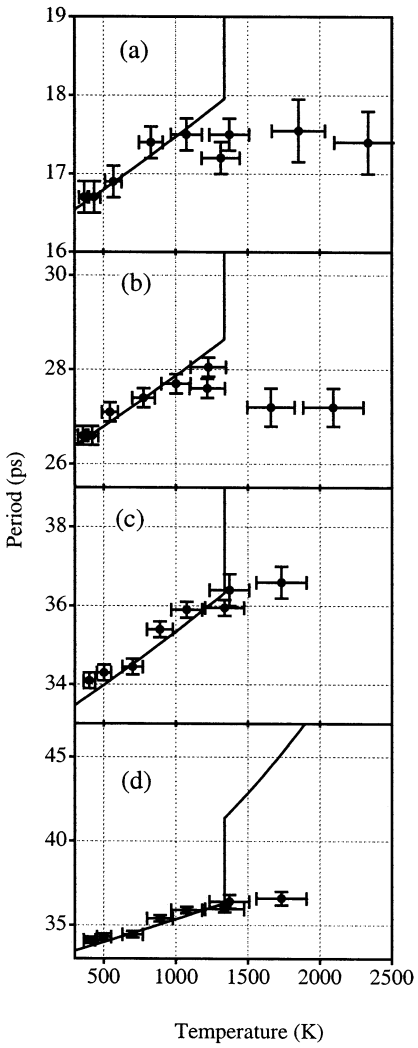

Figure 4. Period versus temperature for the different gold colloid solutions: (a) 50 nm diameter particles; (b) 80 nm diameter particles; (c) 100 nm diameter particles; (d) data for the 100 nm diameter particles presented over a wider scale. The solid lines represent the periods calculated from the temperature-dependent elastic constants of gold (see the text for details).

$$T = T_{\mathrm{m}} + \frac{q - \Delta H_{\mathrm{fus}} - \int_{T_0}^{T_{\mathrm{m}}} C_p(\mathrm{s})\,\mathrm{d}T}{C_{\mathrm{p}}(\mathrm{l})}. \qquad (2b)$$

Equation 2a gives the temperature rise below the melting point ($T_{\mathrm{m}} = 1338$ K), and eq 2b gives the temperature rise above the melting point. The values of the different parameters used were $C_p(\mathrm{s}) = 23.81 + 0.0050T$ J K^{-1} mol^{-1} for solid gold,[49] $\Delta H_{\mathrm{fus}} = 12.4$ kJ mol^{-1},[49] and $C_p(\mathrm{l}) = 29.3$ J K^{-1} mol^{-1} for liquid gold.[50]

To calculate the amount of heat deposited into the particles, we need to know the absorption at 400 nm. This is not a trivial calculation because the extinction spectra presented in Figure 1 arise from both absorption and scattering. The magnitude of the extinction coefficient was determined by comparison to the experimental data in refs 39 and 40, and the relative contributions from absorption and scattering for the differently sized particles were calculated using the full Mie theory expressions.[46,47] The results for the absorption coefficient at 400 nm are $\alpha_{400} = 2000 \pm 100$ M^{-1} cm^{-1} for the 50 nm diameter particles, $\alpha_{400} = 1800 \pm 100$ M^{-1} cm^{-1} for the 80 nm particles, and $\alpha_{400} = 1500 \pm 100$ M^{-1} cm^{-1} for the 100 nm particles. The dielectric constant of the medium used in these calculations was 1.33,[46] and the dielectric constants of gold were taken from ref 51. Note that eq 1 assumes that the absorption of the sample follows Beer's law, which is not correct at powers $I_{\mathrm{o}} > 3-4$ μJ/pulse. This means that the actual temperatures in the particles at high powers are less than those indicated in Figure 4. Unfortunately, it is extremely difficult to quantify the degree of pump laser saturation in this system.

4. Discussion

4.1. Period versus Temperature. Previous work by our group and Vallee and co-workers has shown that for spherical particles the vibrational modes can be accurately described by continuum mechanics.[18,19] The period for the symmetric breathing mode (which is the one excited in our time-resolved experiments) is given by[52,53]

$$\tau_R = 2\pi R/\eta c_{\mathrm{l}} \qquad (3)$$

where c_{l} is the longitudinal speed of sound, R is the radius, and η is an eigenvalue. In Lamb's original derivation the value of η is determined by the first root of the equation $\eta \cot \eta = 1 - (\eta c_{\mathrm{l}}/2c_{\mathrm{t}})^2$, where c_{t} is the transverse speed of sound.[52] This derivation does not take into account surface stress γ. Including surface stress yields the following eigenvalue equation:

$$\eta \cot \eta = 1 - \frac{\eta^2}{4}\frac{c_{\mathrm{l}}^{\,2}}{c_{\mathrm{t}}^{\,2} - \gamma/(2\rho R)} \qquad (4)$$

where ρ is the density of the sphere. For most solids with nanometer-sized dimensions c_{l}^2, $c_{\mathrm{t}}^2 >> \gamma/(2\rho R)$, so the surface stress term can be neglected in eq 4 and the period is solely determined by c_{t} and c_{l} (i.e., η is given by Lamb's equation). However, inclusion of surface stress is important for liquid particles, where the transverse speed of sound c_{t} vanishes; see below.

Calculations of the period versus temperature using eqs 3 and 4 are included in Figure 4. Below the melting point the temperature dependence of the period arises from the temperature dependence of c_{l} and c_{t}. This was calculated using data from ref 54, which is tabulated between 0 and 800 K. Values of c_{l} and c_{t} above 800 K were obtained by extrapolation. Both c_{l} and c_{t} scale linearly with temperature, which means that the eigenvalue value η is only weakly temperature dependent, and the main effect on the period is the decrease in c_{l} with temperature. This causes the approximately linear increase in the period with temperature shown in Figure 4. Note that the assumption that c_{l} and c_{t} change linearly with temperature up to $T \approx T_{\mathrm{m}}$ is consistent with experimental data for Al, Zn, and Cd.[54] Like gold, these metals have close-packed face-centered-cubic structures and, therefore, form a reasonable basis for comparison.

Above the melting point we will assume that gold behaves like an ideal compressible fluid, so that we can set $c_{\mathrm{t}} = 0$.[20] In this case eq 4 can be written as

$$\eta \cot \eta = 1 + \frac{\eta^2}{2}\frac{1}{\epsilon} \qquad (5)$$

where $\epsilon = \gamma/\rho R c_{\mathrm{l}}^2$. Since $\epsilon << 1$, eq 5 can be formally expanded to give

$$\eta = \pi + (2/\pi)\epsilon + O(\epsilon^2) \approx \pi \qquad (6)$$

Thus, the period is simply given by

$$\tau_R = 2R/c_l(l) \quad (7)$$

where $c_l(l)$ is the longitudinal speed of sound in liquid gold. The speed of sound in liquid gold is $c_l(l) = 2560 - 0.55(\Delta T)$ ms^{-1}, where ΔT is the temperature above the melting point.[50] This is significantly different from the longitudinal speed of sound in solid gold, which we estimate to be $c_l(s) = 3050$ ms^{-1} at the melting point.[54] This is the major reason for the discontinuity in the calculated periods in Figure 4 at the melting point of gold. Such abrupt deviations in the material properties at the phase transition point between a solid and liquid are well-known.[50] The estimated 20% decrease in c_l on going from solid to molten gold at T_m is also consistent with the experimentally measured changes for Al, Zn, and Cd.[50,54]

The reasonable agreement between the calculated and experimental periods at temperatures less than ~1300 K shows that our temperature estimates are reliable at pump laser powers below 2 μJ/pulse. At higher pump laser powers (>3 μJ/pulse) the experimental and calculated periods deviate quite dramatically. Note that this is also the point where nonlinear effects start to be significant in the pump beam transmission. The deviation between the calculated and experimental periods indicates that we have not been able to completely melt the particles under our experimental conditions, since a phase transition should be observed as a discrete jump in the period due to the change in material properties.

There are three possible reasons why we cannot achieve melting: (i) At pump laser powers >3 μJ/pulse the pump laser absorption is saturated; i.e., absorption does not follow Beer's law. This means that the actual number of photons absorbed is less than that calculated using eq 1. The 400 nm pump pulses primarily excite the 5d → 6sp interband transition. At high excitation levels, a significant fraction of the 6sp levels will become populated and a significant number of 5d levels will be depleted during the pump laser pulse—leading to a decrease in the absorption. (ii) Melting in materials takes a finite time; that is, for the particles to have the elastic response of liquid gold, the positions of the ions must be disordered ("liquidlike"). The amount of displacement that must occur is determined by the Lindemann criterion for melting. That is, solids melt when the root-mean-square displacement of the nuclei becomes ~1/10 of the average interatomic distance.[50] It is not clear how long this will take in our system, but it will certainly not be instantaneous. (iii) Heat dissipation to the environment limits the temperatures that can be achieved by pulsed laser excitation.

Of these three possibilities we consider (i) the most likely. First, simulations of liquids show that melting from a lattice typically occurs well within 50 ps.[55] Although this time scale no doubt depends on the material, it seems unlikely that melting would not happen within 100−200 ps for gold particles, discounting (ii). Second, the experimental data recorded at pump powers <2 μJ/ pulse, and our previous work on heat dissipation, indicate that at low pump intensities the temperature should not change significantly during the course of the measurement. At high pump intensities the solvent surrounding the particle will become superheated, and possibly boil due to heat transfer from the particles. However, this should decrease the rate of heat dissipation, which makes (iii) unlikely. In addition, heat dissipation cannot explain the threshold behavior observed in the period versus intensity data. Thus, the most likely reason we cannot melt our particles is saturation of the pump laser absorption.

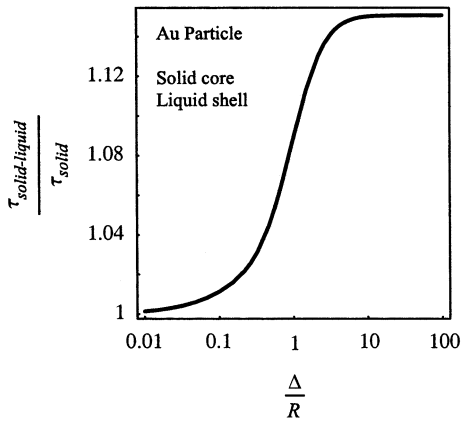

Figure 5. Calculated change in the period of the symmetric breathing mode for a solid-core/liquid-shell Au particle plotted versus the relative thickness of the liquid shell. The vertical axis is the ratio of the period for the solid-core/liquid-shell Au particle $\tau_{solid/liquid}$ to that of a homogeneous solid Au particle τ_{solid}. The horizontal axis is the ratio of the shell thickness Δ to the core radius R.

4.2. Calculations for Solid-Core/Liquid-Shell Particles. It is also relevant at this point to consider whether the particles are partially melted. It is well-known through both simulation[56,57] and experiments[58,59,60] that melting in nanoparticles occurs at the surface, and that significant surface melting can occur at temperatures well below the melting point of the bulk material. For example, surface melting in Pt nanoparticles has been observed at ~600 °C, 1/3 of the bulk melting point for Pt.[61] Thus, it is possible that at high power the particles in our experiments have a solid-core/liquid-shell structure. The period of the symmetric breathing mode in core/shell nanoparticles can be accurately calculated by continuum-mechanics calculations.[62] The predicted increase in the period for a core/shell particle with different thickness liquid shells is presented in Figure 5. In these calculations the speeds of sound in the core were assumed to be $c_t(s) = 1040$ ms^{-1} and $c_l(s) = 3050$ ms^{-1} (i.e., identical to the estimates for solid gold at the melting point) and $c_t(l) = 0$ and $c_l(l) = 2560$ ms^{-1} for the shell (i.e., appropriate for molten gold).

The calculations show that the period increases by <3% for a shell thickness of up to 20% of the total radius. That is, a liquid shell of <20% has very little effect on the period of the symmetric breathing mode. (A change in period of 2−3% is about the sensitivity limit of our experiment.) On the other hand, for liquid shells >75% of the radius, the period is almost exactly the same as that for a pure liquid particle. The change from a response that is essentially the same as that of solid gold to one that is identical to that of molten gold is remarkably abrupt. The experimental results in Figures 3 and 4 show that at high intensities the period is very close to that expected for solid gold at its melting point. Thus, if a liquid shell is formed on the particles, its thickness must be <20% of the radius.

4.3. Damping of the Vibrational Motion at High Temperatures. The last issue examined in this paper is vibrational damping. Figure 6 shows transient absorption data for the 80 nm diameter sample recorded with 0.5 and 5 μJ energy pump laser pulses. The rising background signal (which is clearly evident in Figure 2b, and is much more prevalent at high power) has been subtracted out, and the modulations have been normalized so that their magnitudes are approximately equal at the start of the trace. Also shown in Figure 6 are fits to the normalized data using a damped cosine function. The low-intensity data were fitted using the $S(t) \propto \cos(2\pi t/\tau_R + \phi) \exp[-(\Gamma_\sigma t)^2]$ function, whereas, for the higher intensity data an

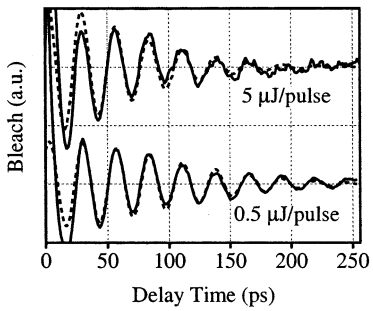

Figure 6. Comparison of transient absorption traces for 80 nm diameter gold particles recorded at high (5 μJ/pulse, top) and low (0.5 μJ/pulse, bottom) pump laser intensities. The modulations are clearly more strongly damped for the high-intensity data. The dashed lines show fits to the data using a damped cosine function (see the text for details).

additional $\exp(-t/\tau)$ decay term was included. The subtraction technique used to remove the rising background signal makes it difficult to accurately fit the modulations and obtain the damping time at high power. However, it is clear from Figure 6 that the modulations at high power are more strongly damped than those at low pump laser power. The results of the analysis of the 0.5 μJ/pulse trace gave $\Gamma_\sigma = 130$ ps^{-1}—which corresponds to a relative standard deviation of 5%. In turn, analysis of the high-intensity data (keeping Γ_σ constant at 130 ps^{-1}) yields a value of $\tau = 150 \pm 50$ ps. Note that fits to the experimental data using a time-dependent period show that there is very little change in the period with time in these experiments. This implies that the changes in material properties and hence temperature are relatively minor during the course of the experiments (as discussed above).

In all our previous experiments the decay of the signal has been attributed to polydispersity in the sample: differently sized particles have different frequency modulations, and the contributions from all the particles produces a damping.[19,29] However, the size distributions should be identical at high and low power; we do not believe that fragmentation is a problem in these experiments. Thus, polydispersity cannot explain the increased damping at high power.

At present we believe that the increased damping may be a signature of liquid-shell formation. A liquid shell could cause damping of the coherent vibrational motion either by viscous damping effects or because different particles have different thickness liquid shells. Specifically, different thickness shells have different periods (as shown in Figure 5), and the variation in period would produce a damping very much like the damping due to polydispersity. Determining whether a liquid shell is in fact formed, and whether this can explain the increased damping of the coherent vibrational motion at high power, will require much more detailed power-dependent experiments than we have currently been able to do.

5. Summary and Conclusions

We have been able to observe softening of the coherently excited breathing mode in colloidal gold particles by performing time-resolved spectroscopy experiments with different intensity pump laser pulses. Large particles (>50 nm in diameter) were chosen for these studies to minimize problems from heat dissipation; larger particles have slower heat dissipation times, which means that the temperature is better defined during the course of the experiments. The results show that the period of the breathing mode increases with pump laser power up to powers of 2−3 μJ/pulse. At higher powers the period versus intensity data flatten off.

The temperature in the particles was estimated from the laser spot size, the absorbance of gold at the pump laser wavelength (assuming that the particles obey Beer's law), and the heat capacity and enthalpy of fusion of the gold. This allows us to compare the measured periods to values calculated from the temperature-dependent elastic constants of solid and liquid gold. The calculated and measured periods are in reasonable agreement up to the melting point of gold, which is predicted to occur at pump laser powers of ~3 μJ/pulse. At higher powers the calculated periods are much longer than the measured periods; an abrupt change in the measured periods is not observed. This indicates that we do not actually achieve temperatures higher than the melting point in these experiments. This is most likely due to saturation of the sample absorption. On the other hand, analysis of the damping of the coherently excited vibrational motion indicates that we may form a liquid shell on the particles at high pump laser power. On the basis of the measured vibrational periods, and calculations of the period expected for solid-core/liquid-shell particles, the thickness of this shell (if present) must be less than 20% of the total radius of the particle.

Acknowledgment. The work described in this paper was supported by the United States National Science Foundation by Grant No. CHE98-16164, and by the Particulate Fluids Processing Centre of the Australian Research Council.

References and Notes

(1) Faraday, M. *Philos. Trans. R. Soc. London* **1857**, *147*, 145.
(2) Mirkin, C. A.; Letsinger, R. L.; Mucic, R. C.; Storhoff, J. J. *Nature* **1996**, *382*, 607.
(3) He, L.; Musick, M. D.; Nicewarner, S. R.; Salinas, F. G.; Benkovic, S. J.; Natan, M. J.; Keating, C. D. *J. Am. Chem. Soc.* **2000**, *122*, 9071.
(4) Martin, B. R.; Dermody, D. J.; Reiss, B. D.; Fang, M. M.; Lyon, L. A.; Natan, M. J.; Mallouk, T. E. *Adv. Mater.* **1999**, *11*, 1021.
(5) Dickson, R. M.; Lyon, L. A. *J. Phys. Chem. B* **2000**, *104*, 6095.
(6) Nicewarner-Pena, S. R.; Freeman, R. G.; Reiss, B. D.; He, L.; Pena, D. J.; Walton, I. D.; Cromer, R.; Keating, C. D.; Natan M. J. *Science* **2001**, *294*, 137.
(7) Francois, L.; Mostafavi, M.; Belloni, J.; Delouis, J. F.; Delaire, J.; Feneyrou, P. *J. Phys. Chem. B* **2000**, *104*, 6133.
(8) Battaglin, G.; Calvelli, P.; Cattaruzza, E.; Polloni, R.; Borsella, E.; Cesca, T.; Gonella, F.; Mazzoldi, P. *J. Opt. Soc. Am. B* **2000**, *17*, 213.
(9) Zhang, J. Z. *Acc. Chem. Res.* **1997**, *30*, 423.
(10) Link, S.; El-Sayed, M. A. *J. Phys. Chem. B* **1999**, *103*, 8410.
(11) El-Sayed, M. A. *Acc. Chem. Res.* **2001**, *34*, 257.
(12) Hodak, J. H.; Henglein, A.; Hartland, G. V. *J. Phys. Chem. B* **2000**, *104*, 9954.
(13) Voisin, C.; Del Fatti, N.; Christofilos, D.; Vallee, F. *J. Phys. Chem. B* **2001**, *105*, 2264.
(14) Del Fatti, N.; Vallee, F. *Appl. Phys. B* **2001**, *73*, 383.
(15) Elsayed-Ali, H. E.; Norris, T. B.; Pessot, M. A.; Mourou, G. A. *Phys. Rev. Lett.* **1987**, *58*, 1212.
(16) Schoenlein, R. W.; Lin, W. Z.; Fujimoto, J. G.; Eesley, G. L. *Phys. Rev. Lett.* **1987**, *58*, 1680.
(17) Sun, C. K.; Vallee, F.; Acioli, L. H.; Ippen, E. P.; Fujimoto, J. G. *Phys. Rev. B* **1994**, *50*, 15337.
(18) Del Fatti, N.; Voisin, C.; Chevy, F.; Vallee, F.; Flytzanis, C. *J. Chem. Phys.* **1999**, *110*, 11484.
(19) Hodak, J. H.; Henglein, A.; Hartland, G. V. *J. Chem. Phys.* **1999**, *111*, 8613.
(20) Pollard, H. F. *Sound Waves in Solids*; Pion: London, 1977.
(21) Nisoli, M.; De Silvestri, S.; Cavalleri, A.; Malvezzi, A. M.; Stella, A.; Lanzani, G.; Cheyssac, P.; Kofman, R. *Phys. Rev. B* **1997**, *55*, 13424.
(22) Hodak, J. H.; Henglein, A.; Hartland, G. V. *J. Phys. Chem. B* **2000**, *104*, 5053.
(23) Perner, M.; Gresillon, S.; Marz, J.; von Plessen, G.; Feldmann, J.; Porstendorfer, J.; Berg, K. J.; Berg, G. *Phys. Rev. Lett.* **2000**, *85*, 792.
(24) Hartland, G. V.; Hu, M.; Wilson, O.; Mulvaney, P.; Sader, J. E. *J. Phys. Chem. B* **2002**, *106*, 743.
(25) Grant, C. D.; Schwartzberg, A. M.; Norman, T. J.; Zhang, J. Z. *J. Am. Chem. Soc.* **2003**, *125*, 549.
(26) Krauss, T. D.; Wise, F. W. *Phys. Rev. Lett.* **1997**, *79*, 5102.
(27) Thoen, E. R.; Steinmeyer, G.; Langlois, P.; Ippen, E. P.; Tudury, G. E.; Cruz, C. H. B.; Barbosa, L. C.; Cesar, C. L. *Appl. Phys. Lett.* **1998**, *73*, 2149.

(28) Cerullo, G.; De Silvestri, S.; Banin, U. *Phys. Rev. B* **1999**, *60*, 1928.
(29) Hartland, G. V. *J. Chem. Phys.* **2002**, *116*, 8048.
(30) Kurita, H.; Takami, A.; Koda, S. *Appl. Phys. Lett.* **1998**, *72*, 789.
(31) Kamat, P. V.; Flumiani, M.; Hartland, G. V. *J. Phys. Chem. B* **1998**, *102*, 3123.
(32) Takami, A.; Kurita, H.; Koda, S. *J. Phys. Chem. B* **1999**, *103*, 1226.
(33) Chang, S. S.; Shih, C. W.; Chen, C. D.; Lai, W. C.; Wang, C. R. C. *Langmuir* **1999**, *15*, 701.
(34) Fujiwara, H.; Yanagida, S.; Kamat, P. V. *J. Phys. Chem. B* **1999**, *103*, 2589.
(35) Ah, C. S.; Han, H. S.; Kim, K.; Jang, D. J. *J. Phys. Chem. B* **2000**, *104*, 8153.
(36) Link, S.; Burda, C.; Nikoobakht, B.; El-Sayed, M. A. *J. Phys. Chem. B* **2000**, *104*, 6152.
(37) Link, S.; El-Sayed, M. A. *J. Chem. Phys.* **2001**, *114*, 2362.
(38) Hodak, J. H.; Henglein, A.; Giersig, M.; Hartland G. V. *J. Phys. Chem. B* **2000**, *104*, 11708.
(39) Henglein, A.; Meisel, D. *Langmuir* **1998**, *14*, 7392.
(40) Henglein A. *Langmuir* **1999**, *15*, 6738.
(41) Hu, M.; Hartland, G. V. *J. Phys. Chem. B* **2002**, *106*, 7029.
(42) Christofilos, D.; Voisin, C.; Del Fatti, N.; Vallee, F. *High-Pressure Res.* **2002**, *22*, 277.
(43) Hodak, J. H.; Martini, I.; Hartland, G. V. *J. Phys. Chem. B* **1998**, *102*, 6958.
(44) Safonov, V. P.; Shalaev, V. M.; Markel, V. A.; Danilova, Y. E.; Lepeshkin, N. N.; Kim, W.; Rautian, S. G.; Armstrong, R. L. *Phys. Rev. Lett.* **1998**, *80*, 1102.
(45) Enüstün, B. V.; Turkevich, J. *J. Am. Chem. Soc.* **1963**, *85*, 3317.
(46) Kreibig, U.; Vollmer, M. *Optical Properties of Metal Clusters*; Springer: Berlin, 1995.
(47) van de Hulst, H. C. *Light Scattering by Small Particles*; Dover Publications: New York, 1981.
(48) Link, S.; Mohamed, M. B.; El-Sayed, M. A. *J. Phys. Chem. B* **1999**, *103*, 3073.
(49) *American Institute of Physics Handbook*, 3rd ed.; McGraw-Hill: New York, 1972.
(50) Iida, T.; Guthrie, R. I. L. *The Physical Properties of Liquid Metals*; Clarendon Press: Oxford, 1988.
(51) Johnston, P. B.; Christy, R. W. *Phys. Rev. B* **1972**, *6*, 4370.
(52) Lamb, H. *Proc. London Math. Soc.* **1882**, *13*, 189.
(53) Bullen, K. E.; Bolt, B. A. *An Introduction to Seismology*, 4th ed.; Cambridge University Press: Cambridge, 1985.
(54) Simmons, G.; Wang, H. *Single-Crystal Elastic Constants and Calculated Aggregate Properties: A Handbook*; The MIT Press: Cambridge, 1971.
(55) Allen, M. P.; Tildesley, D. J. *Computer Simulations of Liquids*; Claredon Press: Oxford, 1999.
(56) Cleveland, C. L.; Luedtke, W. D.; Landman, U. *Phys. Rev. B* **1999**, *60*, 5065.
(57) Qi, Y.; Cagin, T.; Johnson, W. L.; Goddard, W. A. *J. Chem. Phys.* **2001**, *115*, 385.
(58) Buffat, P.; Borel, J.-P. *Phys. Rev. A* **1976**, *13*, 2287.
(59) Lewis, L. J.; Jensen, P.; Barrat, J.-L. *Phys. Rev. B* **1997**, *56*, 2248.
(60) Lereah, Y.; Kofman, R.; Penisson, J. M.; Deutscher, G.; Cheyssac, P.; Ben David, T.; Bourret, A. *Philos. Mag. B* **2001**, *81*, 1801.
(61) Wang, Z. L.; Petroski, J. M.; Green, T. C.; El-Sayed, M. A. *J. Phys. Chem. B* **1998**, *102*, 6145.
(62) Sader, J. E.; Hartland, G. V.; Mulvaney, P. *J. Phys. Chem. B* **2002**, *106*, 1399.